Three-Dimensional Printing of Honeycomb Microwave Absorbers: Feasibility and Innovative Multiscale Topologies

Vincent Laur, Maalouf Azar, Alexis Chevalier, Fabrice Comblet

Three-Dimensional Printing of Honeycomb Microwave Absorbers: Feasibility and Innovative Multiscale Topologies

Vincent Laur, *Senior Member, IEEE*, Azar Maalouf, Alexis Chevalier, and Fabrice Comblet

***Abstract*—In this article, we propose to apply 3-D printing technology to the design and realization of honeycomb microwave absorbers. First, printability of simple honeycomb structures, made of a lossy dielectric material, was evaluated and validated by measurement in the 2–18 GHz frequency band. Effective dielectric properties of honeycomb structures with different dimensions are also discussed. Then, the interest of 3-D printing technology was highlighted by the design, fabrication, and measurement of a multiscale honeycomb absorber that can significantly increase the relative bandwidth. The 3-D printed honeycomb absorbers are compared with others technologies. The potential of this technology was also illustrated by the fabrication and measurement of a pyramidal honeycomb absorber that demonstrates an absorption level of more than 22.9 dB over the 2–18 GHz frequency band.**

***Index Terms*—Composite materials, electromagnetic wave absorption, microwave measurement, three-dimensional (3-D) printing.**

I. Introduction

THE DESIGN and development of lightweight wideband microwave absorbers is an important objective both for industrial and academic laboratories. Polymer composites (especially those made of an elastomeric matrix) are usually used as electromagnetic (EM) wave absorbers. These absorbers are thus constituted of a polymer matrix filled with conductive particles (carbon black, carbon nanotubes, graphene) [1]–[3] or lossy magnetic particles (iron, ferromagnetic alloys, ferrites) [4]–[6]. However, this solution leads the absorbers to be quite heavy, especially at low frequencies, and is thus not compatible with aircraft applications.

In this context, honeycomb microwave absorbers (HCA) offer many advantages. Their mass-to-mechanical strength ratio is potentially very useful. They are also capable of high power handling due to their honeycomb structure that allows heat dissipation by optimizing convection. These absorbers are commonly used in aircraft, below spiral antennas, or as an alternative to standard pyramidal foams in anechoic chambers dedicated to high power measurements. Absorption levels of HCA (regular hexagon) is linked to the radius of the cell a, to the thickness of the cell h, to the thickness of the wall p, and to the EM properties of the materials (see Fig. 1). Due to the asymmetry of the cell, three different directions are defined in order to describe its absorption or dielectric properties: L-, W-, and H-directions with respect to the direction of the electric field.

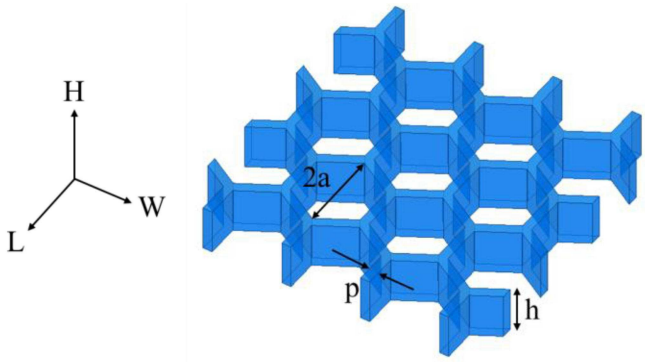

Fig. 1. Three-dimensional view of HCA with their geometrical parameters.

Usually, these HCA are fabricated using aramid or glass fiber paper. This article is then impregnated with a phenolic resin mixed with absorbing particles (e.g., carbon black, carbon nanotubes, etc.) in order to increase losses and induced EM absorption properties. An extrusion process is sometimes used to realize resin honeycombs (HC) in a single step. Unfortunately, these standard fabrication processes do not allow easy study of the effect of geometrical parameters (shape and dimensions of the cell) on microwave absorption properties. For this reason, most publications have focused on the optimization of composition and thickness of the coating layer [7], [8].

Additive technologies are flexible manufacturing processes that make it possible to make complex objects cheaply and seem to be well suited to the fabrication of honeycomb microwave absorbers. Indeed, 3-D printing of lossy materials that can be used as rectangular waveguide loads has already been demonstrated [9]–[12]. This shaping technique has also been used to fabricate free space absorbers [13], [14]. The use of 3-D printing for the fabrication of HCA thus seems possible and can offer numerous advantages [15].

This work was supported by the French Defense Agency(DGA) and the French Research Agency (ANR) in the framework of 3DRAM project.

Vincent Laur, Azar Maalouf, and Alexis Chevalier are with the Lab-STICC Laboratory, University of Brest, 56100 Brest, France (e-mail: vincent.laur@univ-brest.fr; azar.maalouf@univ-brest.fr; alexis.chevalier@univ-brest.fr).

Fabrice Comblet is with the Lab-STICC, ENSTA Bretagne, 29806 Brest, France (e-mail: fabrice.comblet@ensta-bretagne.fr).

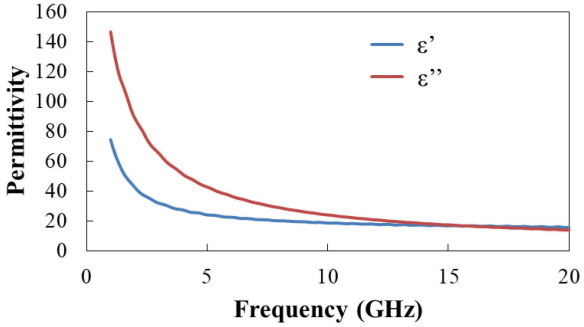

Fig. 2. Permittivity spectrum of PLA-C between 1 and 20 GHz.

In this article, we studied the printability of HCA and new topologies that benefit from the 3-D printing process. We first detail the material properties and fabrication process. Then, we describe how EM properties of HCA were investigated in C-band. Finally, we present the EM modeling of different structures validating the concept by free space measurements.

II. Technologies and Materials

This article was based on the use of fused deposition modeling (FDM), one of the most common and cheap additive technologies. In this technique, a thermoplastic filament is guided in a print head heated at a temperature higher than the melting (crystalline or semi crystalline materials) or glass transition (amorphous materials) temperature of the polymer. The print head moves in the xOy plane while the bed on which the polymer is deposited moves along the z-axis. The object is fabricated layer-by-layer with typical thickness of a single layer between 50 and 300 μm.

In this study, we used a polylactic acid (PLA) filled with carbon particles. This material will be referred to as PLA-C in the following sections of this manuscript. A 3-D printer (3NTR A4v3) was used to shape this material, with the following parameters: nozzle temperature = 190 °C, bed temperature = 65 °C, thickness layer = 200 μm. EM properties of PLA-C were measured by a coaxial probe method (Keysight 85070E Performance Probe) intended for the characterization of liquids but also appropriate for the characterization of flat lossy bulk materials. A cubic bulk sample (50 × 50 × 50 mm) was printed and polished in order to minimize the air gap between the sample and the probe. Fig. 2 presents the evolution of the real and imaginary part of the permittivity of PLA-C in the 1–20 GHz frequency band. The strong dispersion of the imaginary part of the permittivity is typical for a polymer filled with carbon. The decrease of the imaginary part ε" as a function of frequency is proportional to $1/\omega$ and linked to the influence of its macroscopic conductivity. From a value of 74 at 1 GHz, the real part of the permittivity ε' decreases to 15.8 at 20 GHz. In the 1–20 GHz frequency band, dielectric losses (ε"/ε') are very high, with values between 2.1 and 0.9.

III. Printability of HCA

First, we investigated the printability of HCA using PLA-C. Fig. 3 shows different samples of 3-D printed HCA. After

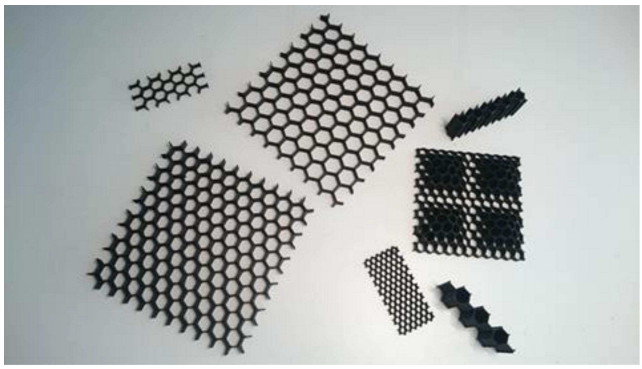

Fig. 3. Examples of HCA samples printed by using PLA-C.

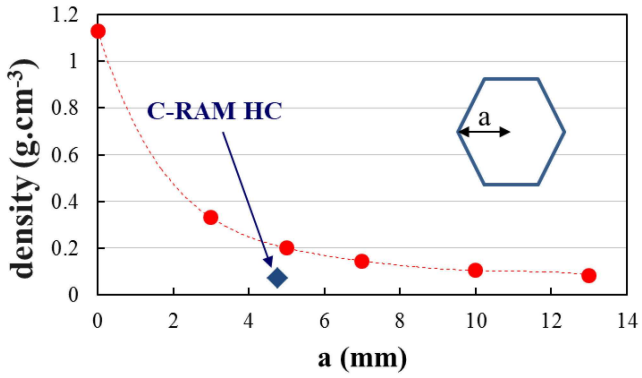

Fig. 4. Evolution of measured density of printed HCA as a function of cell radius a (red circles). Density of a C-RAM HC from cuming microwave (blue diamond).

optimization of printing parameters, it was demonstrated that reproducible HCA with dimensions up to 20 × 20 cm can be fabricated. The main limitation is the minimal thickness of the wall p, which has to be at least 0.8 mm thick due to the nozzle diameter (0.4 mm) of the 3-D printer.

Densities of 3-D printed HCA were measured as a function of the cell radius a for a constant thickness wall $p = 0.8$ mm (see Fig. 4). The density of bulk PLA-C is 1.13 g.cm^{-3}. The increase of the cell radius obviously leads to a decrease of the HCA density, which goes below 0.1 g.cm^{-3} for a cell radius higher than 10 mm. For comparison purposes, a commercial HCA from Cuming Microwave (C-RAM HC) [16], fabricated using aramid fiber paper impregnated with a phenolic resin, has a density of 0.072 g.cm^{-3} for a cell radius of 4.76 mm (see Fig. 4). For similar cell radii, FDM technology thus leads to HCA 2.9 times heavier than those obtained by classical technologies. Depending on the intended application, this characteristic may need to be taken into consideration. However, FDM-printed HCA have better mechanical properties (rigidity) than those made of fiber paper.

In addition to density, the cost of samples is also a crucial aspect for industrial applications. The cost of a 500 g PLA-C spool is currently 78€. The realization of a 15 × 15 cm sample ($a = 10$ mm, $p = 0.8$ mm, $h = 10$ mm) requires a filament of length 4.65 m. Taking into account the density of bulk PLA-C, the mass of this sample would be 34.1 g. The cost of the raw material will thus be very low (5.3€). However, this cost does

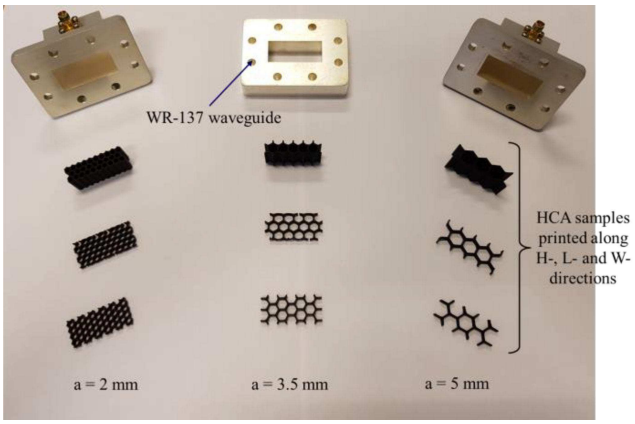

Fig. 5. C-band rectangular waveguide measurement cell and printed HCA samples under test (a is the radius of the cell).

not take into account additional costs such as human resources and printer amortization.

Moreover, one should note that 3-D printing is quite a slow fabrication technique. Although printing speeds are rapidly increasing with the emergence of new FDM printers, the fabrication time of such a sample is still around 3 h. For now, this new technology thus appears to be more suited to the fabrication of small coupling samples rather than absorbers to cover large surfaces.

IV. EM Properties of Printed HCA

Due to shape effects, honeycomb absorbers have inherently anisotropic dielectric properties. In order to investigate dielectric properties of printed HCA, a transmission-reflection method was used. Scattering parameters (S-parameters) of a C-band rectangular waveguide (standard WR-137) loaded with the sample under test were measured and analyzed by a Nicolson–Ross–Weir procedure [17], [18], modified by Baker-Jarvis [19] under the approximation of the propagation of a unique TE_{10} mode. Three different HCA samples were printed for each cell radius under test (a = 2, 3.5, 5 mm) in order to put the direction of electric field parallel to the three inherent directions of HCA cell so that permittivity tensor could be extracted (Fig. 5).

Fig. 6 presents the measured real and imaginary parts of permittivity of a printed HCA with a cell radius a = 5 mm along the W-, L-, and H-directions between 5.85 and 8.2 GHz. The permittivities $\varepsilon_{\mathrm{WW}}$ and $\varepsilon_{\mathrm{LL}}$ are very similar, demonstrating an in-plane isotropy of this cell. $\varepsilon_{\mathrm{HH}}$ is different, however, with a real part value around 40% higher than $\varepsilon_{\mathrm{WW}}$ and $\varepsilon_{\mathrm{LL}}$. One should observe a noticeable dispersion of the dielectric properties (both real and imaginary parts) in the frequency band of measurement due to the strongly dispersive properties of PLA-C.

At 6.5 GHz, the complex permittivity tensor of this sample is

$$\begin{bmatrix} \varepsilon_{WW} & 0 & 0 \\ 0 & \varepsilon_{LL} & 0 \\ 0 & 0 & \varepsilon_{HH} \end{bmatrix}$$

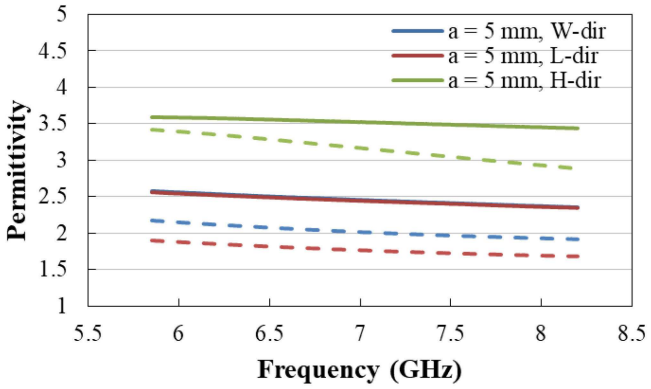

Fig. 6. Real (solid line) and imaginary (dashed line) parts of the permittivity of printed HCA (a = 5 mm) along the three main directions of the unit cell in the 5.85–8.2 GHz frequency band.

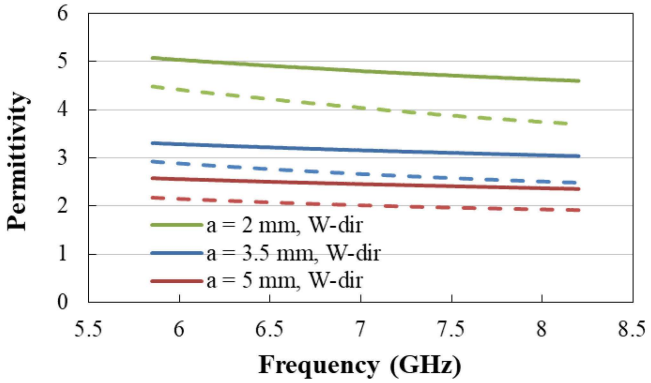

Fig. 7. Real (solid line) and imaginary (dashed line) parts of the permittivity of printed HCA (along W-direction) for three different cell radii in th e 5.85–8.2 GHz frequency band.

$$= \begin{bmatrix} 2.50 - j2.07 & 0 & 0 \\ 0 & 2.49 - j1.82 & 0 \\ 0 & 0 & 3.56 - j3.29 \end{bmatrix} \cdot \quad (1)$$

Dielectric losses range between 0.73 and 0.92 depending on the direction. A slight difference of losses along W- and L-directions was observed, but can be due to measurement uncertainties.

Fig. 7 presents the evolution of the real and imaginary parts of permittivity along the W-direction for three different cell radii. At 6.5 GHz, real part of permittivity is 4.91, 3.22, and 2.50 for cell radii of 2, 3.5, and 5 mm, respectively. Imaginary part of permittivity also decreases with the increasing cell radius. It is thus possible to get different values of permittivity as a function of cell radius intrinsically linked to the air filling ratio.

V. HCA Design

HCA design was realized using finite-element simulation software (Ansys HFSS) in which EM dielectric properties, presented in Fig. 2, were assigned to the material. A unit cell constituted of 16 individual HC cells was simulated with periodic boundaries in order to extract the return loss of the network. It should be noted that the calculated return losses for W- and L-directions

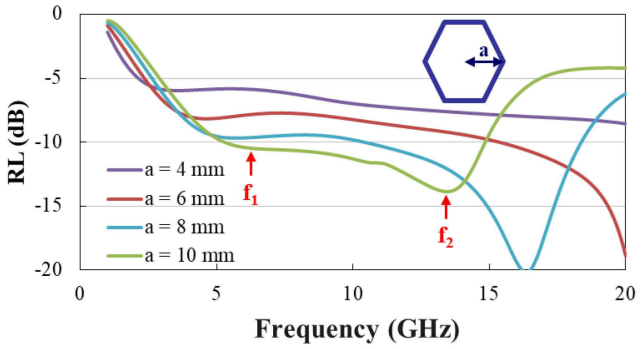

Fig. 8. Simulated L-direction return loss between 1 and 20 GHz as a function of cell radius for a constant thickness $h = 10$ mm and wall thickness $p = 0.8$ mm at normal incidence.

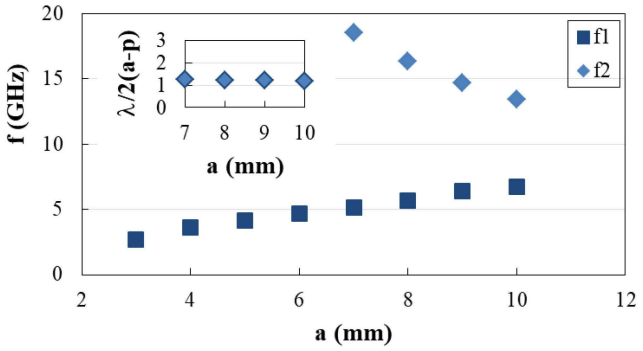

Fig. 9. Evolution of frequencies of maximum absorption level (f_1 and f_2) as a function of cell radius. Inset: wavelength divided by the longest internal dimension of individual HC cells as a function of cell radius for the second absorption peak.

were very similar, so only L-direction will be considered in the following sections of this article. This observation is coherent with the similar measured values of $\varepsilon_{\mathrm{WW}}$ and $\varepsilon_{\mathrm{LL}}$.

Fig. 8 shows return loss at normal incidence of PLA-C HCA for different cell radii but the same thickness $h = 10$ mm and wall thickness $p = 0.8$ mm. Overall, these absorbers present a response with two peaks of absorption at frequencies f_1 and f_2.

In the simulated frequency band, the frequency of the first peak (f_1) increases quite linearly with the increase of cell radius (see Fig. 9). This evolution is typical of an effective medium that behaves as a Dällenbach screen for which a resonance appears when its thickness is equal to a quarter of the guided wavelength $\lambda_g/4$. Indeed, at low frequencies (<7 GHz), guided wavelength is sufficiently high to consider the medium as a homogeneous effective material; other interaction effects between EM wave and HCA can be ignored. For example, a radius $a = 5$ mm lead to a resonance frequency $f_1 = 4.15$ GHz. Inverting this resonance frequency into effective permittivity lead to $\varepsilon_{\mathrm{eff}} = 3.29$ at 4.15 GHz for this HCA. Considering the strong increase in the real part of permittivity at low frequency, this value is coherent with the one measured in C-band for the same HCA.

The second absorption peak appears in the simulated frequency band for radii higher than 6 mm. Its frequency f_2 decreases when the cell radius increases (see Fig. 9). This behavior can be explained by internal reflections inside individual HC

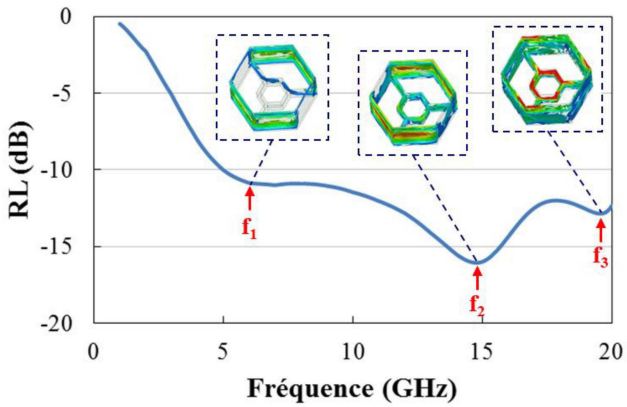

Fig. 10. Return loss of a MS-HCA between 1 and 20 GHz at normal incidence. Inset: electric field amplitude in the cell at different frequencies.

cells. Indeed, for a cell radius of 7 mm, the frequency f_2 is equal to 18.85 GHz. At this frequency, the longest internal dimension of the cell $2(a\text{-}p)$ is very close to the wavelength, thus a dimensional in-plane resonance can occur inside the cell. Moreover, the ratio between wavelength and $2(a\text{-}p)$ remains constant for radius values between 7 and 10 mm, thus demonstrating that the nature of this resonance is the same for this radius range.

Combining these two absorption peaks gives rise to quite a broad bandwidth of absorption for cell radii higher than 8 mm. For a radius of 12 mm, the second peak (f_2) gets too close to the first peak (f_1) cancelling out their effects, then the overall absorption level decreases and leads to a decrease in the bandwidth.

For our experimental demonstrations, a radius of 10 mm was selected to print HCA absorbers. This structure makes it possible to get, in simulation, a return loss level less than –10 dB in the 5.25–14.9 GHz frequency band, and thus, a relative bandwidth of 96% at normal incidence.

Then, we tried to take advantage of the topological freedom allowed by the FDM fabrication technique. A multiscale HCA, referred to hereafter as MS-HCA, was designed. In this structure, the mother cell is an HCA with the following dimensions: $a = 10$ mm, $h = 10$ mm, $p = 0.8$ mm. The addition of a small nested cell, with smaller radius and height ($a = 4$ mm, $h = 3$ mm), inside the mother cell, should improve absorption of the structure.

Fig. 10 shows the simulated return loss of the MS-HCA and electric field pattern, showing the regions where EM energy is located. For frequencies lower than 12 GHz, the return loss is very similar to that of standard HCA; the first absorption peak (f_1) remains unchanged and EM energy is uniformly distributed. The second absorption peak (f_2) is slightly shifted toward higher frequencies ($f_2 = 15$ GHz) and energy concentrates in the walls of the large cell. Then at high frequencies, the additional cell causes a third absorption peak (f_3) at 19.5 GHz. The electric field pattern shows that, at this frequency, the EM energy is concentrated in the walls of the small cell.

Thus, this structure made it possible to extend the bandwidth of absorption up to at least 20 GHz. Experimentally, the upper frequency was limited to 18 GHz due to the limited bandwidth

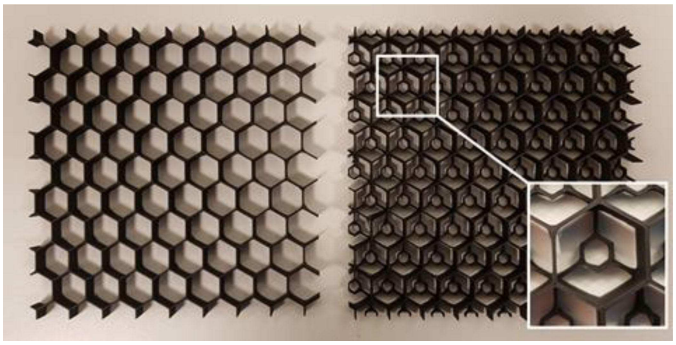

Fig. 11. HCA and MS-HCA printed in PLA-C.

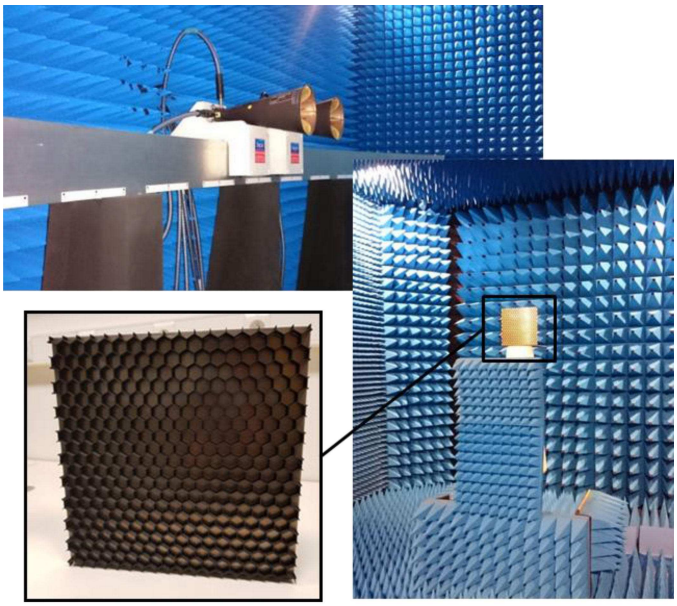

Fig. 12. Measurement setup in the anechoic chamber.

of antennas and absorbers of the anechoic chamber. Considering this maximum frequency, the resulting relative bandwidth was 114%.

VI. Realization and Characterization of 3-D Printed HCA

The HCA and multiscale HCA presented above were fabricated using FDM technology (see Fig. 11). A good agreement between optimized and fabricated dimensions was obtained with, for the simple HCA, a radius $a = 9.85$ mm, a height $h = 10.1$ mm, and a wall thickness $p = 0.78$ mm, which should be compared with the following dimensions considered in the simulated 3-D model: $a_{\mathrm{sim}} = 10$ mm, $h_{\mathrm{sim}} = 10$ mm, $p_{\mathrm{sim}} = 0.8$ mm. HCA and MS-HCA samples were glued on a metallic plate (30 cm $\times$ 30 cm) for the characterization.

These absorbers were measured in an anechoic chamber of dimensions 8 $\times$ 5 $\times$ 5 m ($L \times W \times H$). The distance between the antennas and the measured object was 5 m. Two wideband horns (2–18 GHz) were used to perform bistatic measurements (see Fig. 12). The return loss was obtained as the Radar Cross

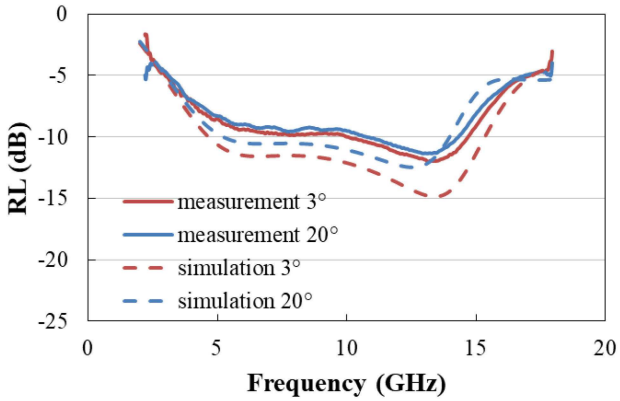

Fig. 13. Comparison of simulated and measured ($\theta = 3°$ and 20°) return loss of HCA for a TE polarized wave.

Section ratio between a metallic plate with and without absorbers. As we knew the exact position of the measured object in the anechoic chamber, a time domain gating around its position could be performed, making the influence of anechoic chamber absorber negligible. Return losses were measured for TE and TM polarizations for quasi-monostatic ($\theta = 3°$) and bistatic ($\theta = 20°$) configurations. Perfect normal incidence ($\theta = 0°$) was not possible in practice due to experimental set-up limitations (the space between horn antennas). Oblique incidence is experimentally limited to 20°.

Fig. 13 compares simulated and measured ($\theta = 3°$ and 20°) return loss (RL) of an HCA for a TE polarized wave. Similar results were obtained for a TM polarized wave. Measured RL show similar trends to the simulated ones with a double peak absorption and moderate variations of absorption between 3° and 20° of incidence. However, a 2 dB degradation of return loss was obtained by measurement compared with simulations, leading to a drastic decrease of –10 dB bandwidth that corresponded to 28% and 40% for TE and TM waves, respectively. However, by taking into account this decrease of absorption, and considering a–8 dB bandwidth, more coherent bandwidths were observed compared with the simulation ($\mathrm{BW_{TE}} = 105\%$, $\mathrm{BW_{TM}} = 103\%$).

The decrease of absorption level is under investigation. This degradation could come from a dispersion of material properties or from edge effects induced by the fabrication of large sample by using four 15 cm $\times$ 15 cm samples glued on the metallic plate.

Fig. 14 compares simulated and measured ($\theta = 3°$ and 20°) return losses of MS-HCA for a TE polarized wave. Unfortunately, as the maximum frequency of wideband horns is 18 GHz, the third peak cannot be observed from these measurements. However, the effect of this third peak is clearly noticeable with a lower level of RL at high frequencies compared with simple HCA. Thus, the measured RL of MS-HCA demonstrate that absorption at high frequencies can be controlled by the inclusion of a small cell inside the mother cell. Return loss remains lower than –10 dB over a bandwidth of 42% and 47% for TE and TM waves, respectively. Considering a –8 dB level, measured bandwidths were in quite good agreement with the simulated ones ($\mathrm{BW_{TE}} = 117\%$ and $\mathrm{BW_{TM}} = 120\%$).

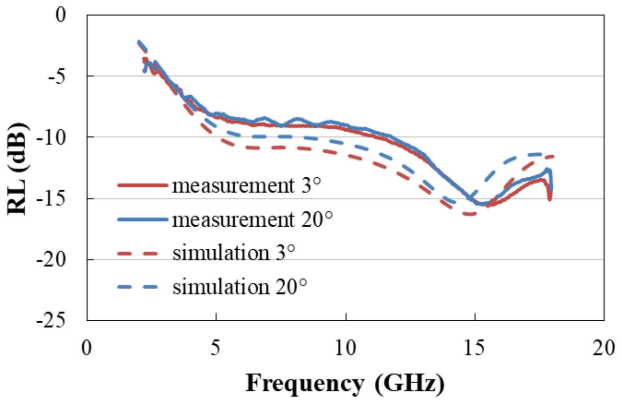

Fig. 14. Comparison of simulated and measured ($\theta = 3°$ and 20°) return loss of MS-HCA for a TE polarized wave.

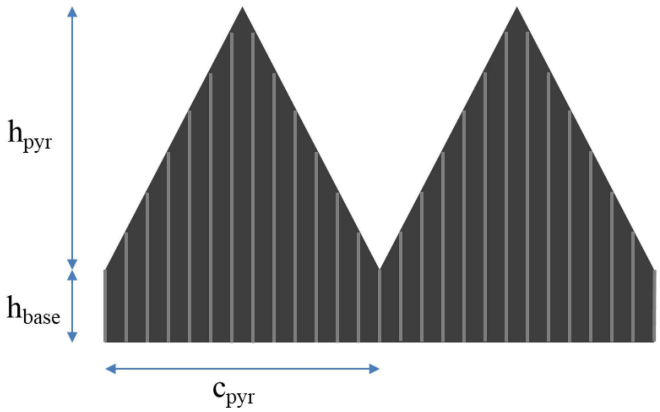

Fig. 15. Dimensions of the studied pyramidal honeycomb absorber.

TABLE I
COMPARISON WITH LITERATURES

Type	Ref.	RBW (%) [X dB]	f_0 (GHz)	Thickness (mm)
MM	[20]	76 [-10]	10	5
MM	[21]	43 [-10]	10.05	2
3D Printed composite	[22]	34.5 [-10]	7.25	5
3D Printed Multilayer MM	[14]	78 [-10]	12.5	7.8
PCB Multilayer MM	[23]	61.6 [-10]	11	5
3D Printed HCA	This work	103 [-8]	12.1	10
3D Printed MS-HCA	This work	117 [-8]	14.9	10

Table I compares our results to different types of microwave absorbers in the same frequency band. Metamaterials (MM) can provide very low profile microwave absorbers to the detriment of relative bandwidth (RBW) [21]. Multilayer multimaterial MM makes it possible to fabricate wideband absorbers [23]. However, such structures usually lead to a quite complex fabrication process that can be overcome by using 3-D printing technology [14]. Our HCA and MS-HCA structures could potentially provide very wideband behavior together with a very simple and cheap fabrication process but return loss levels have to be slightly improved.

VII. Experimental Evaluation of 3-D Printed Pyramidal HCA

To evaluate the potential of this 3-D printing technology at a deeper level, we studied a pyramidal HCA. A commercial pyramidal absorber was selected as a reference (C-RAM SFC-HC-3 from Cuming Microwave) [20] for comparison with the 3-D printing technology. According to the datasheet, this absorber gives a return loss lower than –25 dB at 3 GHz and lower than –38 dB at 18 GHz. To allow a fair comparison between these technologies, the same height was set for the design the printed pyramidal HCA as found in commercial absorbers. The dimensions of the pyramidal HCA were therefore chosen as

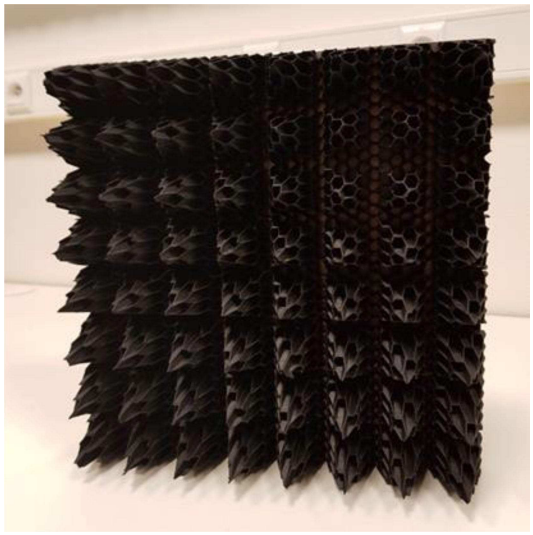

Fig. 16. 3-D printed pyramidal honeycomb absorber.

follows: $h_{\mathrm{pyr}} = 82$ mm, $h_{\mathrm{base}} = 5$ mm, $c_{\mathrm{pyr}} = 37.5$ mm (see Fig. 15). The core of the pyramidal HCA was made of honeycomb cells with a radius of 5 mm and wall thickness of 0.8 mm.

Four similar 15 × 15 cm square samples were printed and glued on a 30 × 30 cm metallic plate (see Fig. 16). It should be noted that the printing time for the fabrication of a single sample is around 23 h.

Fig. 17 compares the simulated and measured return losses of the printed pyramidal HCA for an incidence angle $\theta = 3°$ for TE and TM polarized waves. Simulated return loss is lower than –20.7 dB over the 2–18 GHz frequency band. Slight differences between TE and TM return losses are obtained and could be due to the fact that the pyramid unit cell is not a multiple of the HCA unit cell. Measured return loss is lower than –22.9 dB over the 2–18 GHz frequency band. At 18 GHz, RL remains lower than –48.8 dB for both polarizations. These measurements demonstrate that performance comparable to classical pyramidal HCA can be achieved by using 3-D printing technology and that this technology could pave the way to a new class of absorber

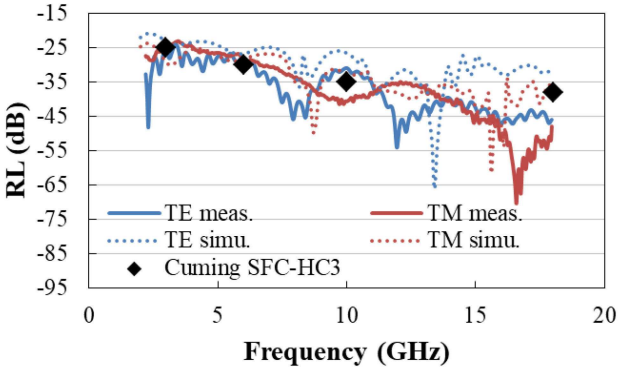

Fig. 17. Return loss of a commercial pyramidal HCA (black diamond [20]) and comparison of simulated and measured return loss of a 3-D printed pyramidal HCA with the same dimensions (blue line: TE polarization, red line TM polarization).

with more complex topologies than the ones achievable with classical technologies (aramid fiber papers, resin impregnation and machining).

VIII. Conclusion

This work demonstrated printability of honeycomb microwave absorbers. The use of carbon-loaded PLA makes it possible to design, fabricate, and characterize HCA, but also multiscale HCA, which cannot be realized by the standard fabrication process. These innovative structures allow an increase in absorption level at high frequencies and, therefore, absorption bandwidth. Pyramidal absorbers were also fabricated and measured. These absorbers show an absorption level of more than 22.9 dB over the 2–18 GHz frequency band, meaning that they offer a similar performance to commercial pyramidal HCA with the same dimensions.

The 3-D printing thus appears as a new way to fabricate low-cost honeycomb absorbers with some limitations: 1) densities of printed HCA are around three times higher than HCA made of aramid fiber paper due to the thicker walls; 2) printing time is quite long. Nevertheless, with the rapid evolution of 3-D printers, these limitations could be overcome in the near future.

Another limitation concerns the polymer matrix that was used in this study. Because the maximum working temperature of PLA is only around 60 °C, this material does not meet the requirements of real-world applications. New polymers and composites with higher operating temperatures [21], [22] dedicated to these applications will therefore need to be investigated for this technology to continue to mature.

References

[1] F. Qin and C. Brosseau, "A review and analysis of microwave absorption in polymer composites filled with carbonaceous particles," *J. Appl. Phys.*, vol. 111, no. 6, 2012, Art. no. 061301.

[2] G. Li, T. Xie, S. Yang, J. Jin, and J. Jiang, "Microwave absorption enhancement of porous carbon fibers compared with carbon nanofibers," *J. Phys. Chem. C*, vol. 116, no. 16, pp. 9196–9201, 2012.

[3] A. Saib *et al.*, "Carbon nanotube composites for broadband microwave absorbing materials," in *Proc. Eur. Microw. Conf. Proc.*, 2005, pp. 1–4.

[4] A. Chevalier and V. Laur, "Composites-based microwave absorbers: Toward a unified model," in *Proc. IEEE Int. Microw. Symp.*, 2017, pp. 1804–1807.

[5] P. Toneguzzo, G. Viau, O. Acher, F. Fiévet-Vincent, and F. Fiévet, "Monodisperse ferromagnetic particles for microwave applications," *Adv. Mater.*, vol. 10, no. 13, pp. 1032–1035, 1998.

[6] J. Neige, T. Lepetit, A. L. Adenot-Engelvin, N. Malléjac, A. Thiaville, and N. Vukadinovic, "Microwave permeability of FeNiMo Falkes-polymer composites with and without an applied static magnetic field," *IEEE Trans. Magn.*, vol. 49, no. 3, pp. 1005–1008, Mar. 2013.

[7] A. Rinaldi, A. Proietti, A. Tamburrano, and M. S. Sarto, "Graphene-coated honeycomb for broadband lightweight absorbers," *IEEE Trans. Electromagn. Compat.*, vol. 60, no. 5, pp. 1454–1462, Oct. 2018.

[8] A. A. Khurram, N. Ali, S. A. Rakha, P. Zhou, and A. Munir, "Optimization of the carbon coating of honeycomb cores for broadband microwave absorption," *IEEE Trans. Electromagn. Compat.*, vol. 56, no. 5, pp. 1061–1066, Oct. 2014.

[9] Y. Arbaoui *et al.*, "Full 3D printed microwave termination: A simple and low cost solution," *IEEE Trans. Micrw. Theory Techn.*, vol. 64, no. 1, pp. 271–278, Jan. 2016.

[10] A. Maalouf, R. Gingat, and V. Laur, "Additive technology applied to the realization of K-band microwave terminations: Reproducibility improvement," *Int. J. Microw. Wireless Technol.*, vol. 10, pp. 3–8, 2018.

[11] Y. Arbaoui, V. Laur, A. Maalouf, and P. Queffelec, "3D printing for microwave: Materials characterization and application in the field of absorbers," in *Proc. IEEE Int. Microw. Symp.*, 2015, pp. 1–3.

[12] A. Pen, A. Chevalier, A. Maalouf, and V. Laur, "X-band compact microwave terminations," in *Proc. IEEE Asia-Pac. Microw. Conf.*, 2018, pp. 315–317.

[13] R. Kronberger and P. Soboll, "New 3D Printed microwave metamaterial absorbers with conductive printing materials," in *Proc. IEEE Eur. Microw. Conf.*, 2016, pp. 596–599.

[14] X. Lleshi, R. Grelot, T. Q. Van Hoang, B. Loiseaux, and D. Lippens, "Wideband metal-dielectric multilayer microwave absorber based on a single step FDM process," in *Proc. IEEE Eur. Microw. Conf.*, 2019, pp. 678–681.

[15] V. Laur, A. Maalouf, A. Chevalier, and F. Comblet, "Study of 3D printed honeycomb microwave absorbers," in *Proc. IEEE Antennas Propag. Symp.*, 2019, pp. 1981–1982.

[16] Cuming Microwave, C-RAM HC. Technical Bulletin 360-1, Mar. 2011. [Online]. Available: https://www.cumingmicrowave.com/pdf/360-Honeycomb & High Power/360-1 C-RAM HC.pdf

[17] A. M. Nicolson and G. F. Ross, "Measurement of the intrinsic properties of materials by time domain techniques," *IEEE Trans. Instrum. Meas.*, vol. IM-19, no. 4, pp. 377–382, Nov. 1970.

[18] W. B. Weir, "Automatic measurement of complex dielectric constant and permeability at microwave frequencies," *Proc. IEEE*, vol. 62, no. 1, pp. 33–36, Jan. 1974.

[19] J. Baker-Jarvis, M. D. Janezic, J. H. Grosvenor, and R. G. Geyer, "Transmission/reflection and short-circuit line methods for measuring permittivity and permeability," Nat. Inst. Stand. Technol., Gaithersburg, MD, USA, Tech. Note 1355-R, Dec. 1993.

[20] F. Costa, A. Monorchio, and G. Manara, "Analysis and design of ultra thin electromagnetic absorbers comprising resistively loaded high impedance surfaces," *IEEE Trans. Antennas Propag.*, vol. 58, no. 5, pp. 1551–1558, May 2010.

[21] S. Ghosh, S. Bhattacharyya, D. Chaurasiya, and K. V. Srivastava, "An ultrawideband ultrathin metamaterial absorber based on circular split rings," *IEEE Antennas Wireless Propag. Lett.*, vol. 14, pp. 1172–1175, 2015.

[22] K. G. Kjelgard, D. T. Wisland, and T. S. Lande, "3D printed wideband microwave absorbers using composite graphite/PLA filament," in *Proc. Eur. Microw. Conf.*, 2018, pp. 859–862.

[23] F. Ding, Y. Cui, X. Ge, and S. He, "Ultra-broadband microwave metamaterial absorber," *Appl. Phys. Lett.*, vol. 100, pp. 103506–103509, 2012.

[24] Cuming Microwave, C-RAM SFC-HC. Technical Bulletin 390-16, Nov. 2012. [Online]. Available: https://www.cumingmicrowave.com/pdf/390-Anechoic Chamber Mat'Is/390-16 C-RAM SFC-HC.pdf

[25] Y. Arbaoui *et al.*, "3D printed ferromagnetic composites for microwave applications," *J. Mater. Sci.*, vol. 52, no. 9, pp. 4988–4996, 2017.

[26] V. Laur, M. Kaissar Abboud, A. Maalouf, D. Palessonga, A. Chevalier, and J. Ville, "Heat-resistant 3D printed microwave devices," in *Proc. IEEE Asia-Pac. Microw. Conf.*, 2018, pp. 1318–1320.